UNIVERSIDADE ESTADUAL DE CAMPINAS
SISTEMA DE BIBLIOTECAS DA UNICAMP
REPOSITÓRIO DA PRODUÇÃO CIENTIFICA E INTELECTUAL DA UNICAMP

Versão do arquivo anexado / Version of attached file:

Versão do Editor / Published Version

Mais informações no site da editora / Further information on publisher's website:
https://www.sciencedirect.com/science/article/pii/S0261306915000527

DOI: 10.1016/j.matdes.2015.02.006

Direitos autorais / Publisher's copyright statement:
©2015 by Elsevier. All rights reserved.

DIRETORIA DE TRATAMENTO DA INFORMAÇÃO

Cidade Universitária Zeferino Vaz Barão Geraldo
CEP 13083-970 – Campinas SP
Fone: (19) 3521-6493
http://www.repositorio.unicamp.br

Materials and Design 72 (2015) 31–42

Contents lists available at ScienceDirect

Materials and Design

journal homepage: www.elsevier.com/locate/matdes

Cooling thermal parameters, microstructure, segregation and hardness in directionally solidified Al–Sn-(Si;Cu) alloys

Felipe Bertelli [a], Crystopher Brito [a], Ivaldo L. Ferreira [b], Guillaume Reinhart [c], Henri Nguyen-Thi [c], Nathalie Mangelinck-Noël [c], Noé Cheung [a,*], Amauri Garcia [a]

[a] Department of Manufacturing and Materials Engineering, University of Campinas – UNICAMP, 13083-970 Campinas, SP, Brazil
[b] Department of Mechanical Engineering, Fluminense Federal University, Av. dos Trabalhadores 420, 27255-125 Volta Redonda, RJ, Brazil
[c] Institut Matériaux, Microélectronique et Nanosciences de Provence, Aix Marseille Université – AMU, 13397 Marseille – Cedex 20, France

ARTICLE INFO

Article history:
Received 29 October 2014
Accepted 14 February 2015
Available online 21 February 2015

Keywords:
Alloys
Solidification
Optical metallography
Microstructure
Hardness

ABSTRACT

The morphology and length scale of the phases forming the microstructure of sliding bearing alloys are known to affect wear, mechanical and corrosion resistances. Al–Sn alloys have good anti-frictional properties due to the presence of Sn. However, with the current trends in engine design, these alloys are not able to support the demanded heavy loads. An alternative way to reach this requirement can be the alloying with third elements such as Si and Cu. Despite the importance of their application properties, studies on the development of microstructures of these multicomponent alloys are rare in the literature. In the present investigation Al–Sn-(Cu;Si) alloys were directionally solidified (DS) under transient heat flow conditions, and a thorough characterization is performed including experimental growth rates and cooling rates, segregation, optical and scanning electron microscopies and primary dendrite arm spacings, λ_1. Experimental growth laws are proposed relating the dendritic spacing to solidification thermal parameters. Furthermore, the scale of the dendritic morphology, the distribution of second phases in interdendritic regions and the macrosegregation pattern are shown to affect the hardness along the length of the DS castings. Hall–Petch type equations are proposed relating hardness to λ_1.
© 2015 Elsevier Ltd. All rights reserved.

1. Introduction

Al-based alloys are extensively used for bearing components, in particular those alloyed with a soft phase such as Pb and Sn [1–13]. Lead has proved to be more effective than tin in aluminium-based sliding bearing materials [14]. However, the increasing environmental concern for Pb has renewed the interest in replacing such element in Al-based alloys for tribological applications with compatible soft alloying elements. Al–Sn alloys have good anti-frictional properties due to the presence of Sn as the soft additive; however, with the increase in engine bearing temperatures associated with recent trends in engine design, these alloys lack their ability to support heavy loads. An alternative way to overcome this problem can be the alloying with a third element such as Si, which is known to increase both the fatigue resistance and the load bearing capacity of the alloy [15–22]. Lastly, copper has also been usually added to bearing alloys with a view to strengthening the aluminium matrix, thus improving mechanical properties and leading to a microstructural combination of strong matrix with dispersed areas of soft Sn phase [23–27]. The mechanical alloying of Mg to Al–Sn alloys was reported to increase the strength and wear performance by improving the distribution of Sn [28].

In the selection of metallic alloys for practical tribological applications, it is important to take into account not only their chemical composition but also the microstructural features that are affected by thermal conditions during casting and by thermal and thermo-mechanical treatments. The effect of the microstructure is more relevant for intimate surface contact, i.e. for practical situations where the use of lubricants is marginal or is not possible. In the microstructural arrangement both the continuity, morphology and distribution of the phases are important. Recent studies highlighted the role of the microstructure length scale on the wear resistance of Al–In [29] and Al–Bi and Al–Pb [30] monotectic alloys. The matrix was shown to provide the required strength while the soft phase acted as a self-lubricant agent. A study by Cruz et al. [31] reported opposite roles of the scale of the dendritic morphology of Al–Sn and Al–Si alloys on the resulting wear resistance. In the case of Al–Si alloys, the refinement of the dendritic array improved the wear resistance, while for Al–Sn alloys lower wear volumes were observed for coarser dendritic structures, which are associated with larger Sn-rich interdendritic regions.

* Corresponding author. Tel.: +55 19 3521 3448; fax: +55 19 3289 3722.
E-mail address: cheung@fem.unicamp.br (N. Cheung).

http://dx.doi.org/10.1016/j.matdes.2015.02.006
0261-3069/© 2015 Elsevier Ltd. All rights reserved.

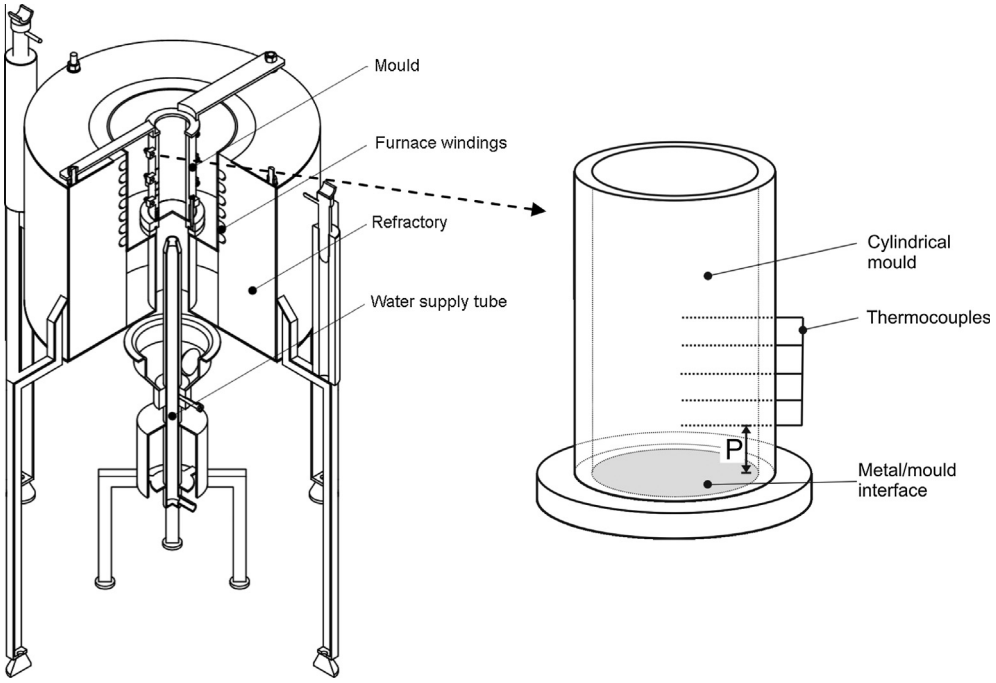

Fig. 1. Schematic vertical upward directional solidification casting assembly and mould details.

Table 1
Chemical composition (wt%) of metals used to prepare the alloys.

Element	Al	Sn	Si	Cu	Fe	Zn	Ni	Pb	Ca
Al	Balance	0.005	0.055	0.010	0.073	0.05	0.006	0.006	–
Sn	0.005	Balance	–	0.004	0.008	–	0.0001	0.047	–
Si	0.110	–	Balance	–	0.320	–	0.010	–	–
Cu	–	–	–	Balance	0.014	–	–	–	0.002

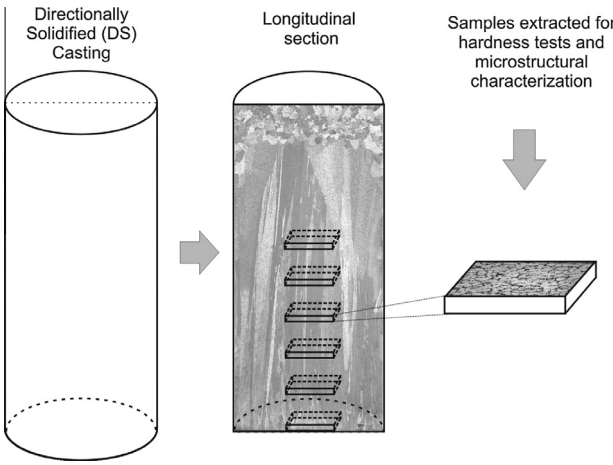

Fig. 2. Sequence used to obtain the samples for microstructural characterization, segregation analysis and hardness tests.

The morphology and length scale of the phases forming the microstructure of sliding bearing alloys were shown to affect also the mechanical and corrosion resistances. For hypoeutectic Al–Sn alloys, the ultimate and yield tensile strengths, as well as the elongation to fracture increased with the decrease in the primary dendrite arm spacing [31]. It was also reported that finer dendritic structures of an Al–10 wt%Sn alloy are associated with lower corrosion rates as compared with coarser dendritic structures [32]. In contrast, recent studies on monotectic Al–In and Al–Bi [33] alloys, which are characterized by microstructures formed by droplets of the minority phase disseminated into the Al matrix, demonstrated that their electrochemical corrosion behaviour is related to the scale of the alloys microstructure. Smaller droplets of the minority phase and smaller interphase spacings were reported to be associated with lower corrosion resistance.

Despite the aforementioned importance of morphology, volumetric fraction, scale, and distribution of the different phases forming the microstructure of metallic alloys on their corresponding application properties, studies on detailed characterization of microstructural features of multicomponent alloys are scarce in the literature due to the difficulty of the task. In addition, most of the solidification experiments are performed under steady state conditions in Bridgman type apparatus [34–40]. On the other hand, directional solidification under transient heat flow conditions is the class of heat flow encompassing the majority of industrial solidification processes [31,32,41–43]. The aim of the present investigation is to analyse the microstructural evolution of ternary Al–Sn-(Si;Cu) alloys under a wide range of cooling rates, using a water-cooled directional solidification system. The parametric features of the microstructures are aimed to be correlated with thermal growth variables such as the growth and the cooling rates with a view to permitting experimental growth laws to be established. The study is also focused on the analysis of macrosegregation effects and on the influence of alloying additions on the scale of the microstructure and hardness.

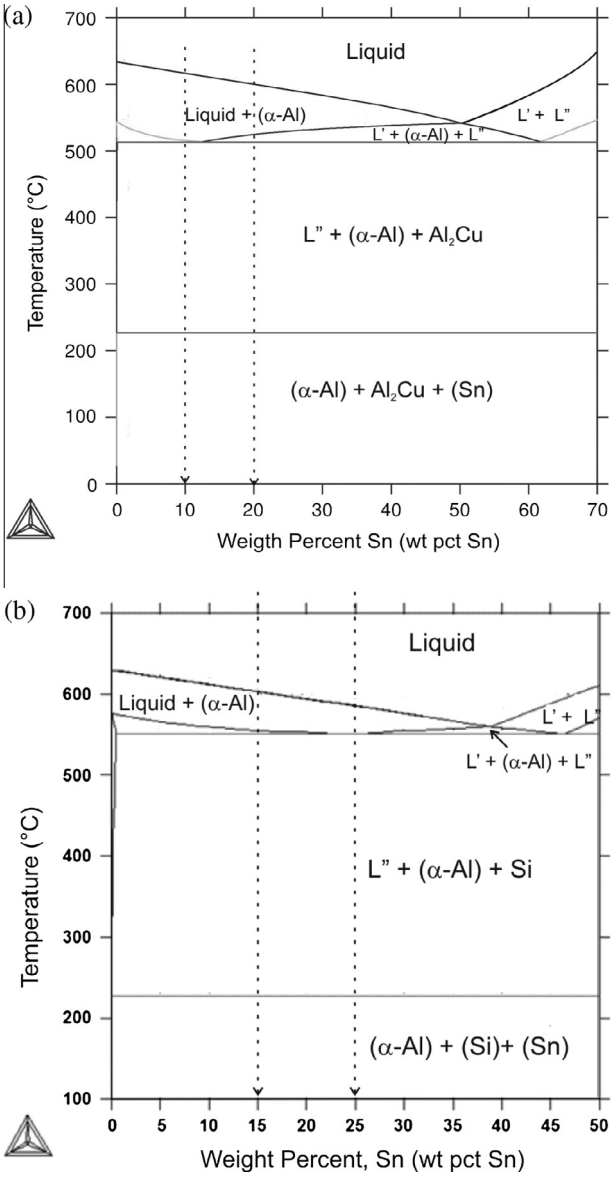

Fig. 3. Pseudo-binary partial phase diagrams of: (a) Al–10 wt%Cu–Sn and (b) Al–5 wt%Si–Sn with indications of the alloys compositions examined in the present study.

2. Experimental

In order to permit a range of solidification microstructures to be obtained at different cooling rates in a single casting experiment, solidification experiments in a water-cooled apparatus (Fig. 1), which promotes transient directional solidification (DS), were performed with ternary Al–Sn–Cu and Al–Sn–Si alloys having the following nominal compositions: Al–10 wt%Sn–10 wt%Cu; Al–20 wt%Sn–10 wt%Cu; Al–15 wt%Sn–5 wt%Si; Al–25 wt%Sn–5 wt%Si. The chemical compositions of metals that were used to prepare these alloys are presented in Table 1.

The DS casting assembly and mould details used in the vertical upward directional solidification experiments (shown schematically in Fig. 1) have been detailed in previous studies [44]. The apparatus consists of a water-cooled mould with heat being extracted only from the bottom, promoting a vertical upward directional solidification. A stainless steel mould was used, having an internal diameter of 50 mm, a height of 110 mm and a wall thickness of 3 mm. The inner vertical surface was covered with a layer of insulating alumina to minimize radial heat losses, thus permitting unidirectional heat flow

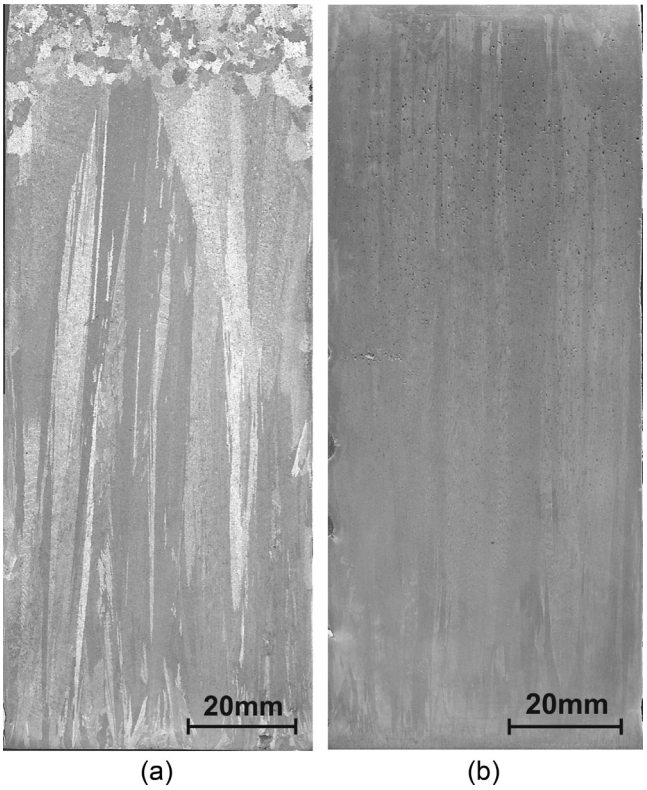

Fig. 4. (a) Macrostructure of the Al–15 wt%Sn–5 wt%Si alloy; (b) macrostructure of the Al–20 wt%Sn–10 wt%Cu alloy.

to be attained. A top cover made of an insulating material was used as a thermal barrier to reduce heat losses at the metal/air surface. The bottom part of the mould was closed with a 3 mm thick carbon steel sheet. As shown in Fig. 1, a set of fine K-type thermocouples, sheathed in 1.6 mm outside diameter (OD) stainless steel tubes, were inserted at different positions from the heat-extracting surface at the bottom of the casting. All the thermocouples were connected by coaxial cables to a data logger interfaced with a computer, capable of autonomously recording temperature data at a frequency of 10 Hz.

The microstructural characterization of the directionally solidified alloys castings was performed by extracting samples at different sections along the castings length, as shown in Fig. 2. The samples were polished with 100, 200, 400, 600, 800 and 1200 grit SiC papers, and then finely polished with diamond paste (1 and 3 μm). The sample surfaces were then subjected to ultrasonic cleaning before etching with a solution of 4% hydrofluoric acid (HF) and 2% hydrochloric acid (HCl) in distilled water. The etching was performed by carefully immersing the samples in the etchant for 10 s, then cleaning the sample surface with running water and ethanol. The optical microscopy was performed using an Olympus Inverted Metallurgical Microscope (model 41GX). The primary dendritic arm spacing (λ_1) was measured from the optical images of the solidified samples (about 40 independent readings for each selected position, with the average taken to be the local spacing).

Square central parts of the transversal samples shown schematically in Fig. 2, were cut by a precision saw into pieces of about 1.0 mm and investigated by a Rigaku Rix 3100 X-ray Fluorescence Spectrometer to estimate their average concentrations through an area of 100 mm^2 probe. This has permitted the occurrence of macrosegregation along the castings length to be investigated.

Vickers hardness tests were performed on transverse sections of the samples, with the measured hardness averaged from at least twenty indentation tests (indentation load of 1 kg and dwell time of 10 s).

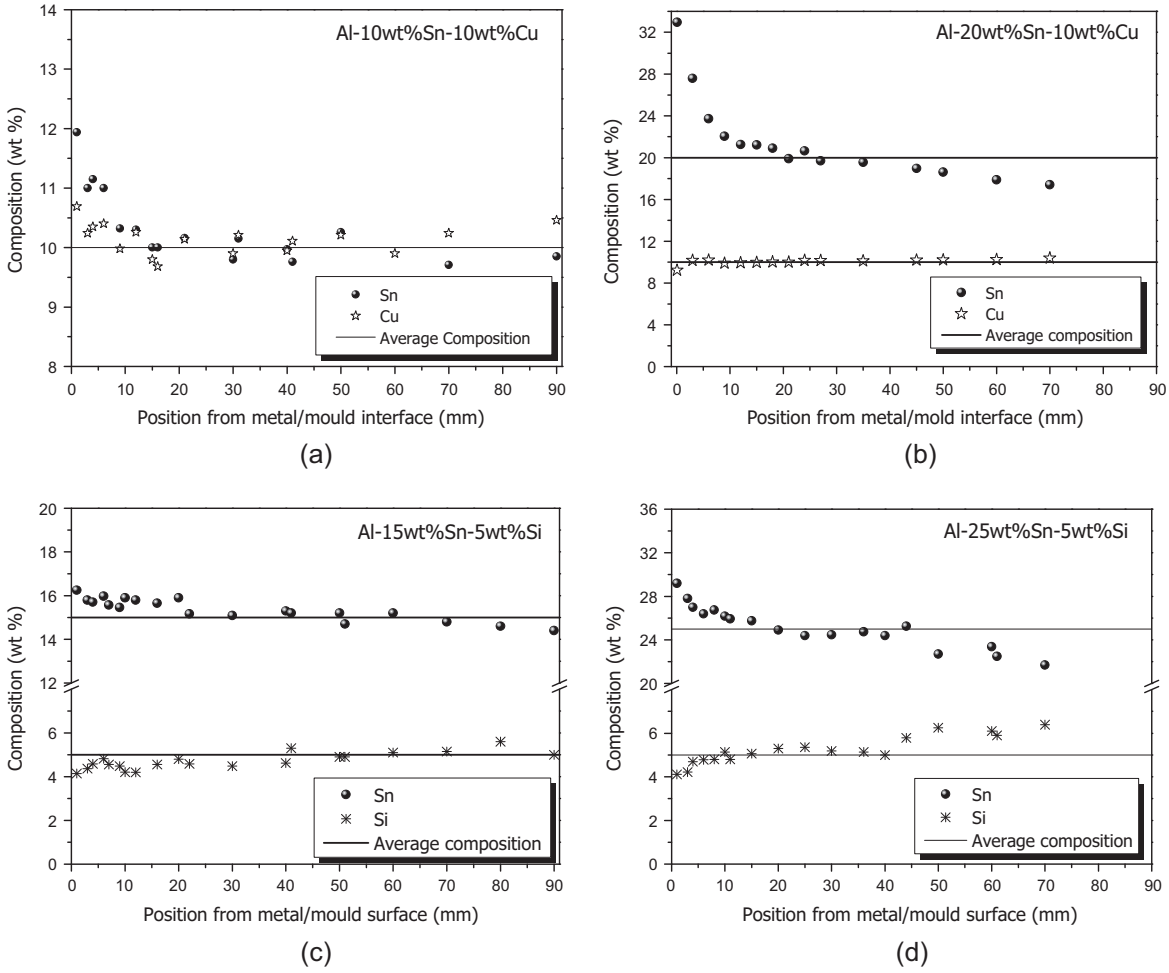

Fig. 5. Experimental solute distribution along the DS castings length of the Al–Sn–Cu and Al–Sn–Si alloys examined in the present study.

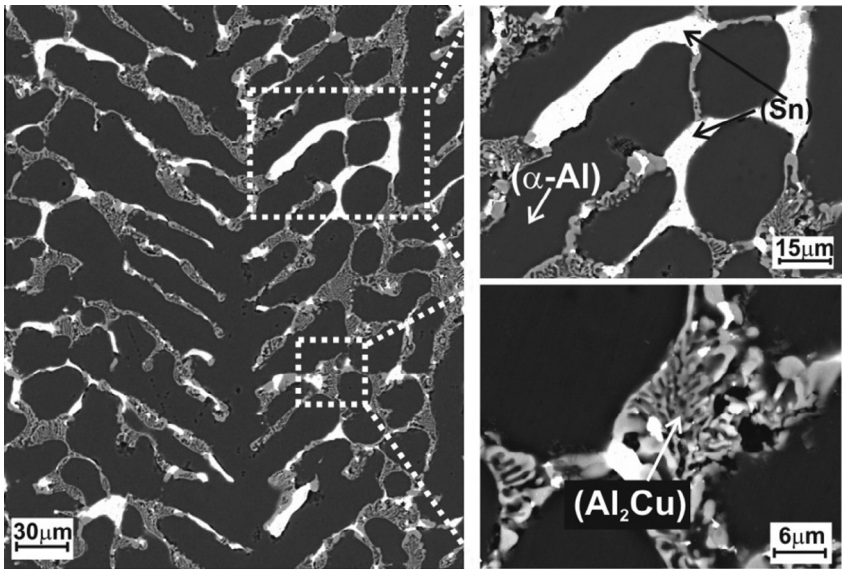

Fig. 6. Typical microstructure of the Al–Sn–Cu alloys examined (SEM images).

3. Results and discussion

The comprehension of solidification paths of Al–Sn(Si;Cu) alloys has scientific and technological interests and are quite complex. The use of computational thermodynamics softwares for a suitable initial characterization of these solidification paths is fundamental [25,45]. In the present study, the solidification paths of two representative Al–Sn–Cu alloys (Al–10 wt%Sn–10 wt%Cu;

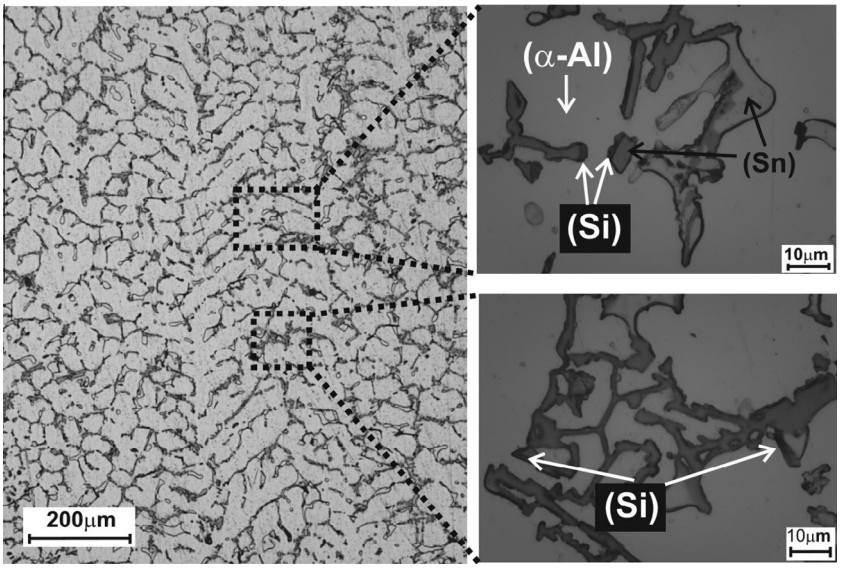

Fig. 7. Typical microstructure of the Al–Sn–Si alloys examined (optical images).

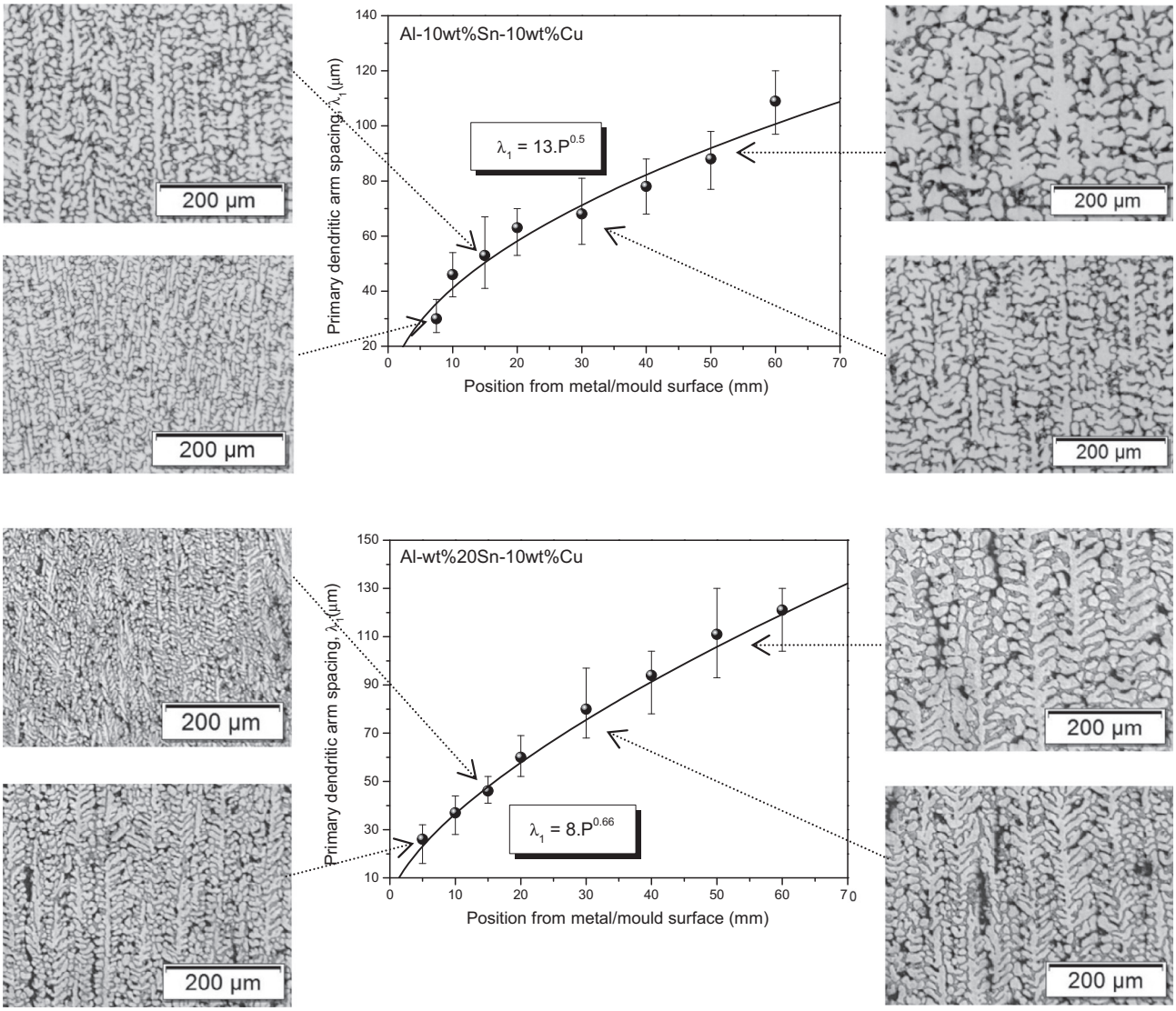

Fig. 8. Evolution of primary dendritic arm spacing (λ_1) as a function of position (P) from the cooled surface of the casting associated with corresponding microstructures.

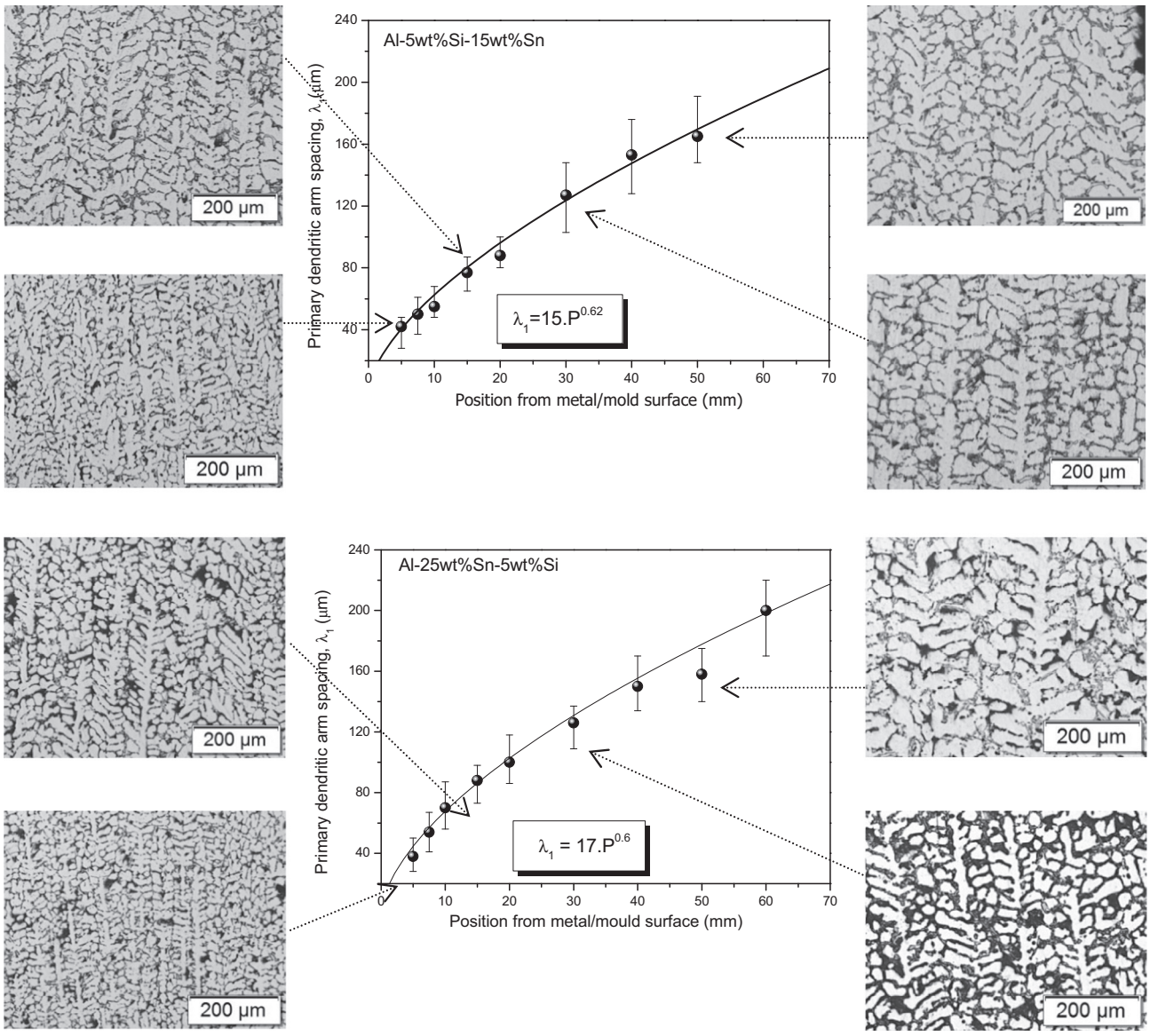

Fig. 8 (*continued*)

Al–20 wt%Sn–10 wt%Cu) have been determined by the use of the Thermo-Calc software. Fig. 3a shows the pseudo-binary diagram corresponding to a parameterized concentration of 10 wt%Cu. The solidification sequences of these alloys are quite similar since these alloys are located outside the miscibility gap, i.e. in the region of primary α-Al solidification. It commences with formation of the α-Al phase. The liquid phase L′ is progressively enriched with Sn until it reaches the boundary of the region of miscibility gap. The liquid L″ starts separation at about 542 °C. A monotectic reaction occurs at 513 °C, where the remaining L′ is transformed (L′ > α-Al + L″ + Al_2Cu). The final L″ liquid is consumed through a eutectic reaction that forms the solid Sn phase (L″ > Sn + α-Al + Al_2-Cu). Detailed analyses combining thermodynamics modelling and experimental studies on a number of Al–Sn–Cu alloys can be found in studies performed by Kotadia et al. [24,25] and Mirković et al. [45].

The solidification paths of Al–Sn–Si alloys are also quite complex and associated with the occurrence of invariant reactions during solidification, but the literature is even scarcer with respect to solidification studies on these ternary alloys. In the present study, the solidification paths of two representative Al–Sn–Si alloys (Al–15 wt%Sn–5 wt%Si; Al–25 wt%Sn–5 wt%Si) have been determined and are shown in Fig. 3b (pseudo-binary diagram corresponding to a parameterized concentration of 5 wt%Si). The phase diagram indicates the presence of a ternary eutectic at about 228 °C. The solidification begins with the formation of initial crystals of the α-Al phase, followed by the binary eutectic reaction (L′ > α-Al + Si). During cooling, a monotectic reaction occurs at 550 °C, where the remaining L′ is transformed (L′ > α-Al + L″ + Si) and with the increase in Sn content, finally the ternary eutectic reaction takes place (L″ > Sn + α-Al + Si). According to a report in the literature, evidences of presence of the ternary eutectic in the resulting microstructure are difficult to be found [15], since it is a difficult task to distinguish phases from binary and ternary eutectic reactions. The binary Sn–Si eutectic reaction occurs at a temperature of about 231.9 °C, which is quite similar to that of pure tin.

Typical macrostructures of Al–Sn–Si and Al–Sn–Cu alloys are shown in Fig. 4a and b, respectively. It can be seen that a columnar structure prevailed along the castings length. The DS castings have been examined along the length with a view to investigating the

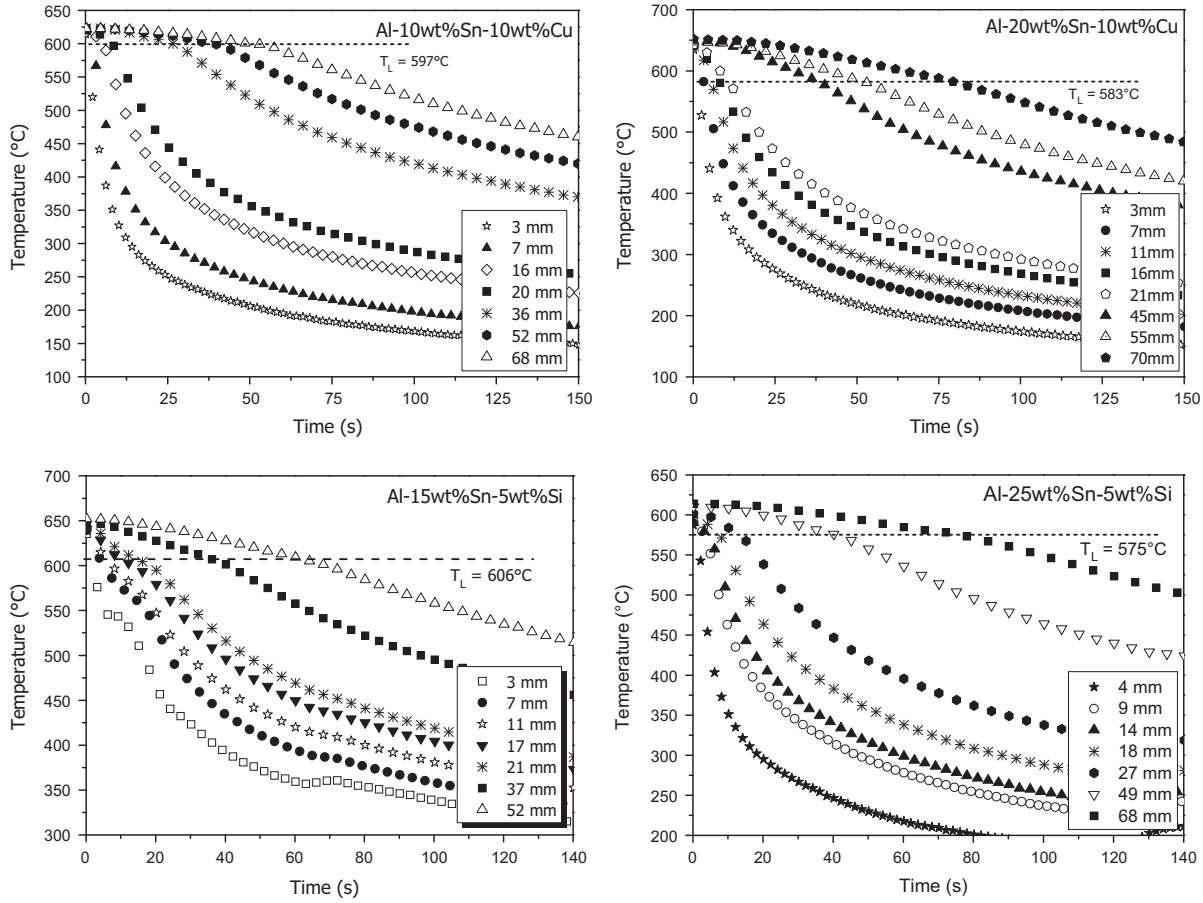

Fig. 9. Temperature data collected by different thermocouples positioned along the castings length during the course of upward directional solidification.

eventual occurrence of long-range segregation. The alloys compositions along the castings length were determined by X-ray fluorescence and are shown in Fig. 5. It can be seen that the Sn distribution along the length of the Al–Sn–Cu castings is characterized by inverse macrosegregation profiles, while the Cu concentration is essentially constant. The literature reports the occurrence of inverse segregation profiles of Sn and Cu in binary Al–Sn [11] and Al–Cu [46] alloys DS castings, respectively. Inverse segregation is commonly associated with long freezing range alloys solidified in chill moulds, which is caused by interdendritic flow of liquid metal induced by solidification shrinkage [47]. A previous study on microporosity formation in an Al–6.2 wt%Cu–1 wt%Si alloy directionally solidified upwards, reported the occurrence of an inverse Cu concentration profile whereas no macrosegregation was observed with respect to the silicon distribution [48]. For the Al–Sn–Si alloys examined in the present study, an inverse Sn segregation profile is only noticeable for the Al–25 wt%Sn–5 wt%Si while Si is essentially constant along the casting length (Fig. 5c and d). Since the DS castings were solidified vertically upwards, it seems that, for both alloys systems, during solidification the high density Sn-rich liquid L″ tends to flow downwards through the interdendritic channels (gravity-driven interdendritic flow) accumulating at the bottom of the casting, thus causing the inverse Sn segregation profiles. It can be seen in Fig. 3a and b that L″ is present along a wide range of temperatures until the final formation of the solid Sn phase.

Fig. 6 shows a typical microstructure of the Al–Sn–Cu alloys, which prevailed along the entire DS casting except for the length scales of the phases. The dendritic morphology of the α-Al phase can be seen with the interdendritic regions formed by segregated Sn pockets (little pools of liquid Sn tend to be caught between dendrite arms) and Al_2Cu intermetallic particles. Fig. 7 shows the typical resulting microstructure observed along the Al–Sn–Si alloys DS castings. It is also characterized by a α-Al phase of dendritic morphology, with both Si particles and segregated Sn pockets in the interdendritic regions.

With a view to characterizing the evolution of the scale of the dendritic morphology along the castings length, the primary dendritic arm spacing (λ_1) was measured from bottom to top of the castings. The resulting experimental values (mean values and error bars representing the range of maximum and minimum experimental measurements) and corresponding microstructures are shown in Fig. 8 as a function of position from the cooled surface of the casting, for any alloy experimentally examined. It is known that the scale of λ_1 depends on the growth conditions, more specifically on thermal parameters such as the local growth rate, thermal gradients and the cooling rate. Both theoretical and experimental [49,50] growth laws relating λ_1 to these parameters can be found in the literature for binary alloys. However, for multicomponent alloys there are no theoretical models available in the literature describing the growth of primary dendritic arms. It is important to have experimental growth laws relating λ_1 to the experimental thermal parameters along the DS of the ternary alloys examined in the present study. This can be done from an appropriate analysis of thermal data during solidification, as subsequently described.

The cooling curves at different positions along the DS castings length are shown in Fig. 9. The thermocouples readings, collected during solidification, were used to generate plots of position (P) from the metal/mould interface as a function of time (t) corresponding to

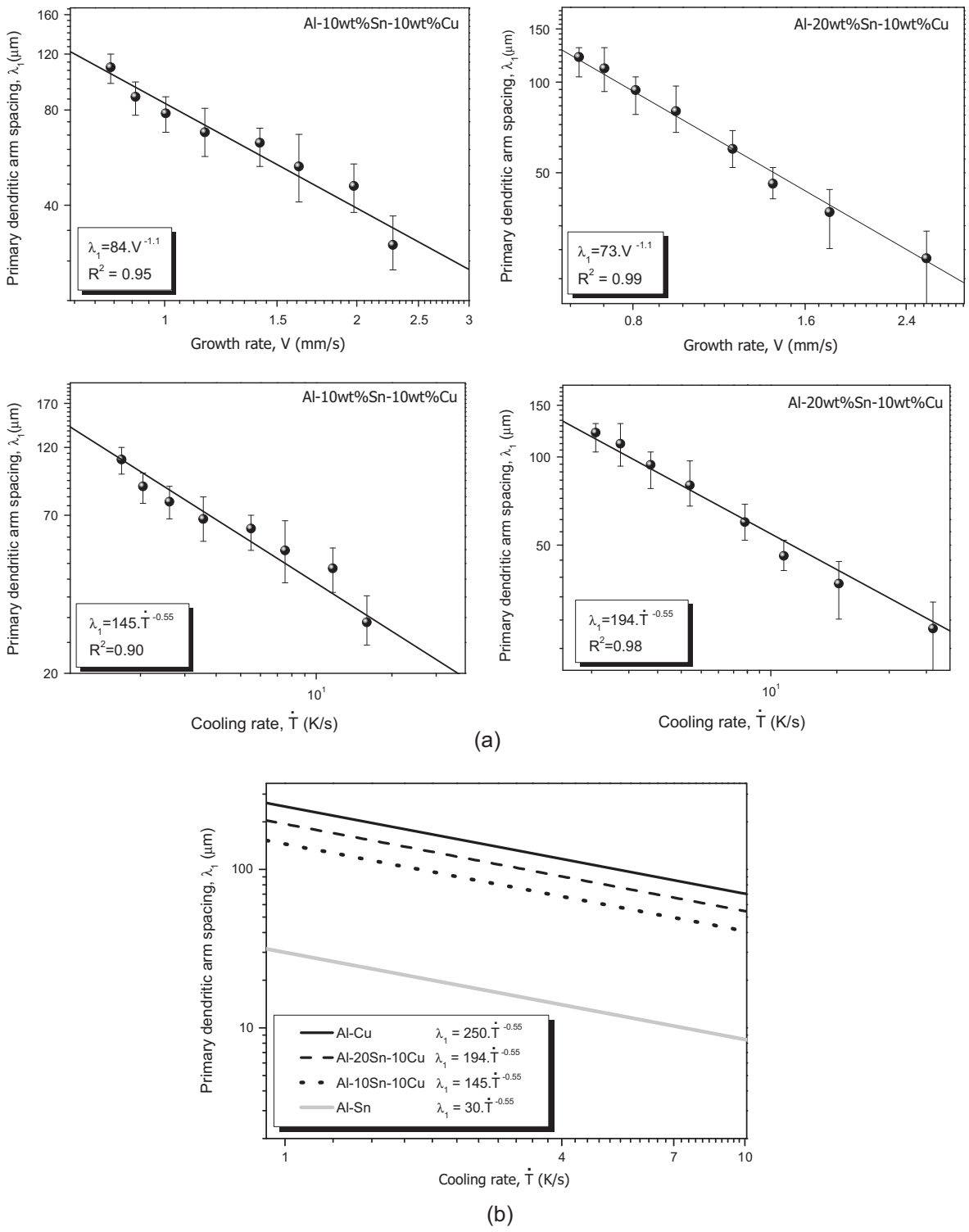

Fig. 10. (a) Primary dendritic arm spacing as a function of growth rate and cooling rate for the directionally solidified Al–Sn–Si alloys (R^2 is the coefficient of determination) and (b) experimental λ_1 vs. $\dot{T}$ laws for the ternary Al–Sn–Cu alloys compared with those determined for Al–Sn [11] and Al–Cu alloys [25].

the *liquidus* front of each alloy passing by each thermocouple. A numerical technique, based on the minimum square method, was used to fit mathematical power functions of the form $P(t) = a\,t^b$ (a; b are constants) on these experimental plots. The derivative of these functions with respect to time gave values for the growth rate (V). Moreover, the data acquisition system employed permitted accurate determination of the slope of the experimental cooling curves. Hence, the cooling rate ($\dot{T}$) was determined along the castings lengths, by considering the thermal data recorded immediately after the passage of the *liquidus* front by each thermocouple.

With a view to permitting correlations between the primary dendritic arm spacing and the growth rate and cooling rate to be established, their experimental values were plotted in Figs. 10a and 11a for the Al–Sn–Cu and Al–Sn–Si alloys investigated in the

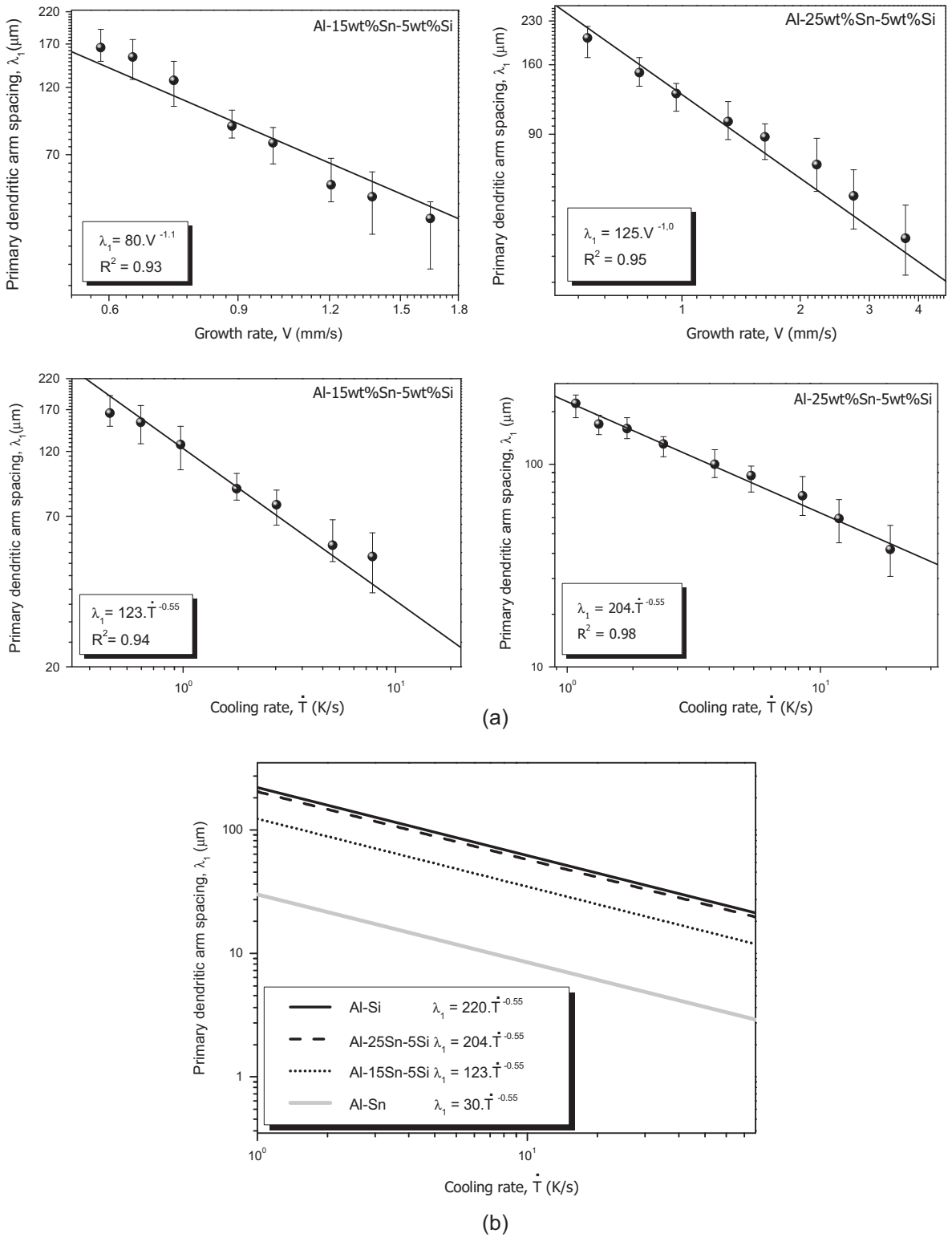

Fig. 11. (a) Primary dendritic arm spacing as a function of growth rate and cooling rate for the directionally solidified Al–Sn–Si alloys (R^2 is the coefficient of determination) and (b) experimental λ_1 vs. $\dot{T}$ laws for the ternary Al–Sn–Si alloys compared with those determined for Al–Sn and Al–Si alloys [11].

present study, respectively. Experimental exponents of (−1.0 to 1.1) and (−0.55) for the power function equations shown in Figs. 10a and 11a, seem to be adequate to characterize the evolution of λ_1 with the growth rate and the cooling rate, respectively, for any alloy examined. These exponents have also been reported to apply to the transient directional solidification of a number of binary metallic alloys [50].

The experimental λ_1 vs. $\dot{T}$ laws for the ternary alloys are compared in Figs. 10b and 11b with those experimentally determined for the corresponding binary alloys, i.e. Al–Sn [31] and Al–Cu [51] and Al–Sn and Al–Si [31], respectively. For both ternary alloys systems the higher is the Sn concentration of the Al–Sn–Cu and Al–Sn–Si alloys, the closer is the λ_1 vs. $\dot{T}$ growth law of the ternary alloy to that of the Al–Cu and Al–Si binary alloys, respectively. The

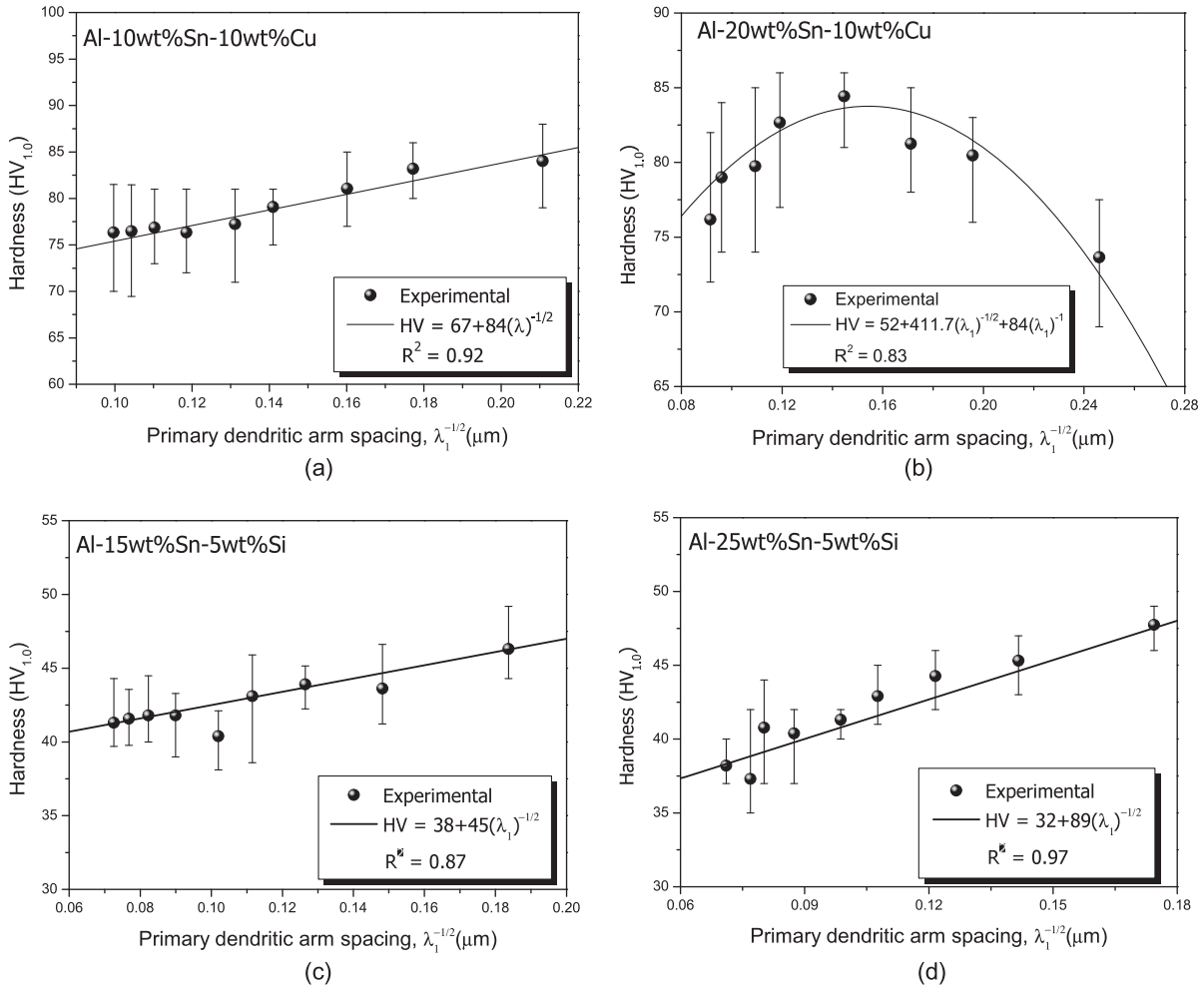

Fig. 12. Vickers hardness (HV) as a function of $\lambda_1^{-1/2}$ for the DS castings of (a); (b) Al–Sn–Cu alloys and (c); (d) Al–Sn–Si alloys.

primary spacing is indeed governed by the formation of the α-Al phase and of the intermetallic Al_2Cu or Si. Sn is mainly implied in the eutectic reactions and interdendritic phases. The theoretical growth models are generally structured to describe a tendency preserving the rationality in the constitutive parameters affecting the scale of the dendritic spacing. However, there are no theoretical growth models in the literature relating λ_1 to solidification thermal parameters for multicomponent alloys. Assuming that, the growth of primary dendritic arms of the ternary alloys indicated in the pseudo-binary diagrams of Fig. 3a and b, could be assessed by an appropriate growth law applicable to the transient solidification of a binary alloy, the Bouchard–Kirkaldy model [49] could be used to analyse the effect of Sn alloying on λ_1. The aforementioned model is given by:

$$\lambda_1 = a_1\left(\frac{16C_0^{1/2}G_0\varepsilon\Gamma D}{(1-k_0)m_L\dot{T}}\right)^{1/2} \quad (1)$$

where C_0 is the alloy composition, $G_0\varepsilon$ is a characteristic parameter $\approx 600 \times 6\ \mathrm{K\,cm^{-1}}$, Γ is the Gibbs–Thomson coefficient, D is the liquid solute diffusivity, k_0 is the solute partition coefficient, m_L is the slope of the liquidus line, and a_1 is the primary dendrite-calibrating factor [49]. Assuming that the liquidus and solidus lines are straight and $k_0 < 1$, m_L is given by:

$$m_L = \frac{\Delta T}{\frac{C_0}{k_0} - C_0} = \frac{\Delta T\ k_0}{C_0(1-k_0)} \quad (2)$$

where ΔT is the difference between the *liquidus* and *solidus* equilibrium temperatures. Comparing Eqs. (1) and (2) we can write:

$$\lambda_1 = a_1\left(\frac{16C_0^{3/2}G_0\varepsilon\Gamma D}{\Delta T\ k_0\dot{T}}\right)^{1/2} \quad (3)$$

According to Eq. (3) λ_1 is inversely proportional to the alloy solidification range and directly proportional to the alloy solute content. That could explain, by analogy, the trend observed for the ternary alloys examined in the present study. For both systems, the alloys having higher Sn content (C_0 in Eq. (3)) have also lower ΔT, considering the range of temperatures in which the dendrites of the α-Al phase are formed. This means that their primary arm spacings would be higher than those of the alloys having lower Sn content for a given cooling rate, as shown by the experimental results in Figs. 10b and 11b for the Al–Sn–Cu and Al–Sn–Si alloys, respectively.

It is well known that microstructural features in large measure determine the mechanical behaviour of alloys. As shown in Figs. 10 and 11 and by the alloys microstructures shown in Figs. 6–8, the cooling rate during directional solidification is shown to affect both the microstructural scale (dendrite arms and particles size) and the distribution of the interdendritic phases. Correlations between parametric features of the as-solidified microstructure can be useful to effect improvements in the associated mechanical strength. With a view to envisaging the role of the scale of the dendritic spacing on mechanical properties, the primary arm spacing has been correlated with local hardness along the DS castings length for all alloys examined in the present study. The experimental results are shown in Fig. 12, with the Vickers hardness (HV) plotted as a function of the square root of λ_1. As can be seen, generally the

smaller the dendritic spacing, the higher HV (Fig. 12a, c and d) and Hall–Petch type formulae are proposed to fit the experimental results. In these cases, the deformation of the α-Al dendritic matrix is significantly constrained (for smaller dendritic spacings) by the more homogeneous distribution of reinforcing Si or Al_2Cu particles in the interdendritic regions, for Al–Sn–Si and Al–Sn–Cu alloys, respectively. This is caused by dislocation pile-up and enhances the resulting hardness, despite the simultaneous occurrence of soft Sn pockets in the interdendritic areas. The exception is the hardness evolution along the DS Al–20 wt%Sn–10 wt%Cu alloy casting, in which hardness has a particular evolution, as shown in Fig. 12b. The hardness is lower for smaller dendritic spacings (at regions close to the cooled surface of the casting), increases up to a maximum value and decreases again with the increase in λ_1 according to a modified Hall–Petch experimental equation, depicted in Fig. 12b. This is caused by the more intense inverse Sn profile that has been experimentally observed for such alloy casting, as shown in Fig. 5b. Outside this region in casting, which is characterized by significant inverse segregation, the evolution of hardness with $\lambda_1^{-1/2}$ has a trend that is similar to those observed for the other alloys examined, i.e. HV decreases with the increase in λ_1.

4. Conclusions

The following conclusions can be drawn from the present experimental investigation:

- The Sn distribution along the length of the Al–Sn–Cu castings is characterized by inverse macrosegregation profiles, while the Cu concentration is essentially constant. For the Al–Sn–Si alloys examined, an inverse Sn segregation profile is only noticeable for the Al–25 wt%Sn–5 wt%Si while Si is essentially constant along the casting length
- The typical microstructure that prevailed along the entire DS casting of the Al–Sn–Cu/Si alloys, is characterized by a dendritic morphology of the α-Al phase, with the interdendritic regions formed by segregated Sn pockets and Al_2Cu/Si particles for the Al–Sn–Cu and Al–Sn–Si alloys, respectively.
- Experimental power function growth laws with exponents of (−1.0 to 1.1) and (−0.55) are proposed to describe the evolution of λ_1 with the growth rate and the cooling rate, respectively, for any alloy examined. For both ternary alloys systems the higher is the Sn concentration of the Al–Sn–Cu and Al–Sn–Si alloys, the closer is the λ_1 vs.$\dot{T}$ growth law of the ternary alloy to that of the corresponding Al–Cu and Al–Si binary alloys, respectively.
- Correlations between the primary dendritic arm spacing with local hardness along the DS castings length permitted Hall–Petch type equations to be proposed relating λ_1 to HV. The smaller λ_1, the higher HV, except for the DS Al–20 wt%Sn–10 wt%Cu alloy casting, in which hardness has a particular evolution caused by a significant inverse profile of segregated Sn associated with regions close to the cooled surface of the casting.

Acknowledgements

The authors acknowledge the financial support provided by FAPESP – São Paulo Research Foundation, Brazil (Grants 2012/08494-0, 2012/16328-2, 2013/23396-7 and 2014/21893-6), CAPES-COFECUB (Grant 857/15), FAEPEX-UNICAMP and CNPq (The Brazilian Research Council).

References

[1] Zhu M, Gao Y, Chung CY, Che ZX, Luo KC, Li BL. Improvement of the wear behaviour of Al–Pb alloys by mechanical alloying. Wear 2000;242:47–53.
[2] Pathak JP, Mohan S. Tribological behaviour of conventional Al–Sn and equivalent Al–Pb alloys under lubrication. Bull Mater Sci 2003;26:315–20.
[3] Noskova NI, Vil'danova NF, Filippov YI, Churbaev RV, Pereturina IA, Korshunov LG, et al. Preparation, deformation, and failure of functional Al–Sn and Al–Sn–Pb nanocrystalline alloys. Phys Met Metallogr 2006;102:646–51.
[4] Ran G, Zhou J, Xi S, Li P. Microstructure and morphology of Al–Pb bearing alloy synthesized by mechanical alloying and hot extrusion. J Alloy Compd 2006;419:66–70.
[5] Wu XF, Zhang GA. Influence of Sn content on the microstructure and dry sliding wear behaviour of hypereutectic Al–20Si alloy. Adv Mater Res 2011;299–300:265–8.
[6] Lu ZC, Zeng MQ, Gao Y, Zhu M. Significant improvement of wear properties by creating micro/nano dual-scale structure in Al–Sn alloys. Wear 2012;296:469–78.
[7] Liu X, Zeng MQ, Ma Y, Zhu M. Promoting the high load-carrying capability of Al–20 wt%Sn bearing alloys through creating nanocomposite structure by mechanical alloying. Wear 2012;294–295:387–94.
[8] Agafii VI, Petrenko VI, Fomichev VM, Yurchenko VI, Yurchenko EV, Dikusar AI. Electrospark alloying for deposition on aluminum surface of Al–Sn coatings and their wear resistance under dry friction. Surf Eng Appl Electrochem 2013;49:181–8.
[9] Bravo AE, Durán HA, Jacobo VH, Ortiz A, Schouwenaars R. Towards new formulations for journal bearing alloys. Wear 2013;302:1528–35.
[10] Feyzullahoğlu E, Ertürk AT, Güven EA. Influence of forging and heat treatment on wear properties of Al–Si and Al–Pb bearing alloys in oil lubricated conditions. Trans Nonferr Met Soc 2013;23:3575–83.
[11] Lu ZC, Zeng MQ, Gao Y, Zhu M. Minimizing tribolayer damage by strength–ductility matching in dual-scale structured Al–Sn alloys: a mechanism for improving wear performance. Wear 2013;304:162–72.
[12] Rusin NM, Skorentsev AL. Improving the tribological properties of self-lubricating Al–Sn alloys by their severe plastic processing. Appl Mech Mater 2013;379:110–4.
[13] Sui B, Zeng JM, Chen P, Liang LH, Gan WK, Lu JB. Study on tribological performance of Al_2O_3 particle reinforced the Al–Sn bearing alloy. Appl Mech Mater 2014;633–634:137–40.
[14] Mittal R, Tomar A, Singh D. Wear behavior of disk shape spray formed Al–Si–Pb alloys. J Mater Eng Perform 2014;23:975–81.
[15] Yuan GC, Li ZJ, Lou YX, Zhang XM. Study on crystallization and microstructure for new series of Al–Sn–Si alloys. Mater Sci Eng, A 2000;280:108–15.
[16] Yuan GC, Zhang XM, Lou YX, Li ZJ. Tribological characteristics of new series of Al–Sn–Si alloys. Trans Nonferrous Met Soc China 2003;13:774–80.
[17] Kong CJ, Brown PD, Harris SJ, McCartney DG. The microstructures of a thermally sprayed and heat treated Al–20 wt%Sn–3 wt%Si alloy. Mater Sci Eng A-Struct 2005;403:205–14.
[18] Pramanick A, Chatterjee S, Bhattacharya V, Chattopadhyay K. Synthesis and microstructure of laser surface alloyed Al–Sn–Si layer on commercial aluminum substrate. J Mater Res 2005;20:1580–9.
[19] Abd El-Salam F, Abd El-Khalek AM, Nada RH, Wahab LA, Zahran HY. Thermally induced structural and mechanical variations in ternary Al–Si based alloys. Mater Sci Eng A-Struct 2009;527:281–6.
[20] Abd El-Salam F, Abd El-Khalek AM, Nada RH, Wahab LA, Zahran HY. Effect of Sn content on the structural and mechanical properties of Al–Si alloy. Mater Sci Eng, A 2010;527:1223–9.
[21] Nada RH, Abd El-Salam F, Abd El-Khalek AM, Wahab LA, Zahran HY. Effect of cyclic stress reduction on the creep parameters of Al–Si alloy with Ag and Sn additions. Mater Sci Eng A-Struct 2012;552:486–92.
[22] Rameshkumara T, Rajendran I. Mechanical and tribological properties on Al–Sn–Si alloy-based plain bearing material. Tribol Trans 2013;56:268–74.
[23] Marrocco T, Driver LC, Harris SJ, McCartney DG. Microstructure and properties of thermally sprayed Al–Sn-based alloys for plain bearing applications. J Therm Spray Technol 2006;15:634–9.
[24] Kotadia HR, Doernberg E, Patel JB, Fan Z, Schmid-Fetzer R. Solidification of Al–Sn–Cu immiscible alloys under intense shearing. Metall Mater Trans A 2009;40A:2202–11.
[25] Kotadia HR, Das A, Doernberg E, Schmid-Fetzer R. A comparative study of ternary Al–Sn–Cu immiscible alloys prepared by conventional casting and casting under high-intensity ultrasonic irradiation. Mater Chem Phys 2011;131:241–9.
[26] Pola A, Montesano L, Gelfi M, Roberti R. Semisolid processing of Al–Sn–Cu alloys for bearing applications. Solid State Phenom 2013;192–193:562–8.
[27] Zhai W, Hu L, Geng DL, Wei B. Thermodynamic properties and microstructure evolution of ternary Al–10%Cu–*x*%Sn immiscible alloys. J Alloy Compd 2015;627:402–9.
[28] Lu ZC, Gao Y, Zeng MQ, Zhu M. Improving wear performance of dual-scale Al–Sn alloys: the role of Mg addition in enhancing Sn distribution and tribolayer stability. Wear 2014;309:216–25.
[29] Freitas ES, Spinelli JE, Casteletti LC, Garcia A. Microstructure-wear behavior correlation on a directionally solidified Al–In monotectic alloy. Tribol Int 2013;66:182–6.
[30] Freitas ES, Silva AP, Spinelli JE, Casteletti LC, Garcia A. Inter-relation of microstructural features and dry sliding wear behavior of monotectic Al–Bi and Al–Pb alloys. Tribol Lett 2014;55:1392–400.
[31] Cruz KS, Meza ES, Fernandes FAP, Quaresma JMV, Casteletti LC, Garcia A. Dendritic arm spacing affecting mechanical properties and wear behavior of Al–Sn and Al–Si alloys directionally solidified under unsteady-state conditions. Metall Mater Trans A 2010;41A:972–84.

[32] Osório WR, Spinelli JE, Cheung N, Garcia A. Secondary dendrite arm spacing and solute redistribution effects on the corrosion resistance of Al–10 wt%Sn and Al–20 wt%Zn alloys. Mater Sci Eng, A 2006;420:179–86.
[33] Osório WR, Freitas ES, Garcia A. Corrosion performance based on the microstructural array of Al-based monotectic alloys in a NaCl solution. J Mater Eng Perform 2014;23:333–41.
[34] Sumida M. Band structure formation in peritectic Fe–Co and Fe–Ni alloys. Mater Trans 2003;44:1351–8.
[35] Ourfali MF, Todd I, Jones H. Effect of solidification cooling rate on the morphology and number per unit volume of primary Mg2Si particles in a hypereutectic Al–Mg–Si alloy. Metall Mater Trans A 2005;36:1368–72.
[36] Li H, Zhao J, Zhang Q, He J. Microstructure formation in a directionally solidified immiscible alloy. Metall Mater Trans A 2008;29:3308–16.
[37] Kaya H, Engin S, Böyük U, Çadırlı E, Maraşlı N. Unidirectional solidification of Zn-rich Zn–Cu hypoperitectic alloy. J Mater Res 2009:3422–31.
[38] Zhang Y, Ma SG, Qiao JW. Morphology transition from dendrites to equiaxed grains for AlCoCrFeNi high-entropy alloys by copper mold casting and Bridgman solidification. Metall Mater Trans A 2012;43:2625–30.
[39] Hu X, Li Y, Liu Y, Min Z. Developments of high strength Bi-containing Sn0.7Cu lead-free solder alloys prepared by directional solidification. J Alloy Compd 2015;625:241–50.
[40] Zhong H, Li S, Kou H, Li J. The solidification path related columnar-to-equiaxed transition in Ti–Al alloys. Intermetallics 2015;59:81–6.
[41] Rohatgi PK, Pasciak K, Narendranath CS, Ray S, Sachdev A. Evolution of microstructure and local thermal conditions during directional solidification of A356–SiC particle composites. J Mater Sci 1994;29:5357–66.
[42] Şahin HM, Kocatepe K, Kayıkcı R, Akar N. Determination of unidirectional heat transfer coefficient during unsteady-state solidification at metal casting–chill interface. Energy Convers Manage 2006;47:19–34.
[43] Kumar A, Dutta P. Numerical studies on columnar-to-equiaxed transition in directional solidification of binary alloys. J Mater Sci 2009;44:3952–61.
[44] Goulart PR, Spinelli JE, Cheung N, Ferreira IL, Garcia A. Cellular growth during transient solidification of hypoeutectic Al–Fe alloys. J Alloy Compd 2009;470:589–99.
[45] Mirković D, Gröbner J, Schmid-Fetzer R. Liquid demixing and microstructure formation in ternary Al–Sn–Cu alloys. Mater Sci Eng, A 2008;487:456–67.
[46] Boeira AP, Ferreira IL, Garcia A. Alloy composition and metal/mold heat transfer efficiency affecting inverse segregation and porosity of as-cast Al–Cu alloys. Mater Des 2009;30:2090–8.
[47] Pickering EJ. Macrosegregation in steel ingots: the applicability of modelling and characterisation techniques. ISIJ Int 2013;53:935–49.
[48] Ferreira IL, Lins JFC, Moutinho DJ, Gomes LG, Garcia A. Numerical and experimental investigation of microporosity formation in a ternary Al–Cu–Si alloy. J Alloy Compd 2010;503:31–9.
[49] Bouchard D, Kirkaldy JS. Prediction of dendrite arm spacings in unsteady and steady-state heat flow of unidirectionally solidified binary alloys. Metall Mater Trans B 1997;28:651–63.
[50] Spinelli JE, Cheung N, Garcia A. On array models theoretical predictions versus measurements for the growth of cells and dendrites in the transient solidification of binary alloys. Philos Mag 2011;91:1705–23.
[51] Rocha OL, Siqueira CA, Garcia A. Heat flow parameters affecting dendrite spacings during unsteady-state solidification of Sn–Pb and Al–Cu alloys. Metall Mater Trans A 2003;34:995–1006.